Environmental Science & Technology

ARTICLE

pubs.acs.org/est

The Red Mud Accident in Ajka (Hungary): Characterization and Potential Health Effects of Fugitive Dust

András Gelencsér,[†] Nóra Kováts,[†] Beatrix Turóczi,[†] Ágnes Rostási,[†] András Hoffer,[‡] Kornélia Imre,[†] Ilona Nyirő-Kósa,[†] Dorottya Csákberényi-Malasics,[†] Ádám Tóth,[†] Aladár Czitrovszky,[§] Attila Nagy,[§] Szabolcs Nagy,[†] András Ács,[†] Anikó Kovács,[†] Árpád Ferincz,[†] Zsuzsanna Hartyáni,[†] and Mihály Pósfai*[,†]

[†]University of Pannonia, Veszprém, Hungary

[‡]Air Chemistry Group of the Hungarian Academy of Sciences, Veszprém, Hungary

[§]Research Institute for Solid State Physics and Optics, Hungarian Academy of Sciences, Budapest, Hungary

Supporting Information

ABSTRACT: As a result of a tragic industrial accident, a highly alkaline red mud sludge inundated settlements and agricultural areas near Ajka, Hungary on October 4, 2010. One of the major concerns about the aftermaths of the accident is the potential health effects of vast amounts of fugitive dust from red mud sediment. Thus, we studied the chemical and physical properties of particles of red mud and its respirable fugitive dust, and performed toxicity measurements. Under unfavorable meteorological conditions dry red mud sediment could emit very high amounts of respirable alkaline particles into the air. The number size distribution of fugitive dust peaks above 1 μm aerodynamic diameter; therefore, its inhalation is unlikely to affect the deep regions of the lungs. No significant mineralogical or elemental fractionation was observed between the sediment and dust, with the major minerals being hematite, cancrinite, calcite, and hydrogarnet. Although the high resuspension potential and alkalinity might pose some problems such as the irritation of the upper respiratory tract and eyes, based on its size distribution and composition red mud dust appears to be less hazardous to human health than urban particulate matter.

INTRODUCTION

On October 4, 2010, following the burst of a containment structure operated by an alumina plant in Ajka, Hungary, about 700,000 m^3 of highly caustic red mud slurry flooded three settlements and about 40 km^2 of agricultural area along the Torna stream and the Marcal river (Supporting Information Figure SI 1). The spill caused the death of 10 persons (some of whom drowned and some who suffered severe burns from the alkaline solution) and major damage to property in the affected area. This catastrophic industrial accident has been unprecedented in the 120-year-long history of the Bayer process.

Red mud is a byproduct of the production of alumina from bauxite in the Bayer process which involves reaction with NaOH at high temperature and pressure. The disposal of red mud raises severe environmental concerns, primarily because of its large volume and highly caustic nature.[1] Even though several schemes have been developed for the practical utilization of red mud, including its use for adsorption of metals from water,[2] the retention of phosphorus in soil,[3] and for CO_2 sequestration,[4] most of the caustic sludge is stored in land-based deposits.[5]

One of the environmental concerns related to red mud is the fact that its fine-grained particles can be released into the atmosphere by wind action. Therefore, the technology of wet storage of red mud prescribes precautionary measures against drying and resuspension, including the recycling and regeneration of the caustic slurry above deposited red mud in containment structures, and covering and recultivation of filled-up disposal sites.

Although the properties and environmental "compatibility" of red mud have been studied extensively,[6,7] the accident at the Ajka alumina plant presents a situation in which conditions significantly differ from those that were present in previous studies. Since vast amounts of caustic red mud cover residential and

Received: November 30, 2010
Accepted: January 14, 2011
Revised: January 13, 2011

agricultural areas, it is no longer possible to prevent drying and resuspension of particles by conventional technology. Outside of its technological storage facilities, massive resuspension of red mud particles may occur, posing unspecified health hazards in the area for a prolonged time. Among all potential mid- to long-term environmental problems, the emission of respirable particulate matter is of primary concern.

The health hazards posed by the respirable fraction of urban particulate matter have been the subject of numerous studies worldwide.[8] However, these results cannot be used directly to assess the adverse health effects of PM_{10} (respirable particulate matter with aerodynamically equivalent particle diameter <10 μm) resuspended from red mud because the released particles are likely highly caustic due to the presence of residual NaOH—a property that is unique in a globally acidic ambient atmosphere. A recently issued Risk Assessment Report on solid NaOH [9] explicitly declares that its atmospheric emission either in gaseous or particulate form is impossible. Further concerns may include the potential presence of other toxic or harmful constituents enriched in the fugitive dust of red mud sediment, including ultrafine particles, needle-like mineral particles, and labile transition metals. The few available studies on the environmental effects and properties of red mud did not indicate significant toxicity or adverse effects of red mud after neutralization,[6,7] but none attempted to assess the health hazard posed by the inhalation of either caustic or neutralized red mud particles. Soils contaminated with industrial chemicals often raise the issue of potential genotoxic effects.[10]

The objective of our study was to comprehensively characterize both the spilled red mud sediment and particulate matter (PM_{10}) resuspended from it with special emphasis on the potential health hazard posed by inhalation of these particles. Besides providing information for local residents and authorities involved in cleanup operations, our results can be relevant for uncovered red mud storage sites worldwide from which fugitive dust is released. The contamination of soil by red mud and its toxicity for plants is discussed in a companion paper.[11]

SAMPLES AND METHODS

Field Sampling. Red mud sediment samples were collected on an agricultural field near Kolontár (SI Figure SI 1) and from an inundated garden in Devecser (Table 1, samples 1 and 4, respectively), and then dried under an infrared lamp for 24 h and used for various measurements (Table 1). The same samples were used for generating aerosol particles in the laboratory using the methods described below. Resuspended PM_{10} dust was collected at three locations in Devecser (Table 1), using a sampler that was developed in our laboratory for collecting the inhalable fraction of resuspended road dust (PM_{10}). The instrument uses a leaf blower to mobilize dust from paved surfaces, simulating very windy conditions (wind speeds ~100 km h^{-1}). The key unit in the apparatus is a PARTISOL-FRM model 2000 sampler that is operated at a flow rate of 16.7 L min^{-1} and contains a cyclone separator which collects the $PM_{(10-1)}$ fraction (particles with aerodynamically equivalent diameters <10 μm but >1 μm) in bulk in a tiny holder. This opens up the possibility of deploying analytical methods which are not suited for the analysis of filter samples. The PM_{10} inlet was connected with a duct system to a preseparator head that excluded debris and giant particles. The PM_1 fraction of the dust was collected on backup filters (Whatman QMA). The sampler is mounted on a mobile platform and powered with a portable electrical power generator. During field sampling an MSP Personal Environmental Monitor, model 200 personal PM_{10} sampler was also operated near the breathing zone of the person operating the road dust sampler (Table 1). This MSP personal sampler collects the total respirable PM_{10} fraction on 37 mm diameter quartz fiber filter at a flow rate of 10 L min^{-1}.

PM_{10} Resuspension Potential of Pulverized Dry Red Mud Sediment. 100 mg of dried and pulverized red mud sediment samples were weighed into a glass flask, then resuspension was performed by blowing N_2 at a flow rate of 7 L min^{-1}. PM_{10} samples were collected with the MSP personal aerosol sampler at a flow rate of 10 L min^{-1} for 5 min. The masses of the PM_{10} fractions were determined gravimetrically, and a mass balance was established.

Determination of the pH and the Alkalinity of the Red Mud Aerosol. An aliquot of the bulk $PM_{(10-1)}$ fraction of resuspended red mud dust was weighed into a 5 mL glass beaker and 2 mL deionized water was added to it. The solution was thoroughly mixed and ultracentrifuged at 4000 L min^{-1}. The pH of the supernatant was measured directly with a pH-meter (Radiometer Copenhagen PHM62). The alkalinity of the samples was calculated directly from the pH-measurements.

Determination of Water-Soluble Metals (Cd, Co, Cu, Ni). 11.40−50.41 mg size-fractionated samples collected in the field (Table 1) were extracted in 2 mL high purity (Milli-Q) water. The solution was filtered through a membrane filter of 0.45 μm pore size, and acidified to pH < 2 with high purity nitric acid. The concentrations of soluble metals were determined by ICP-OES (Perkin-Elmer Optima 2000 DV).

Size Distribution of Resuspended Dust. The mass and number size distributions of dried and resuspended red mud dust were determined in the laboratory in a special all-glass apparatus with an electrical low-pressure impactor (ELPI) that measures particle number concentrations on 12 stages in the size range of 0.03−10 μm, at a flow rate of 30 L min^{-1}. The plates of the impactor were covered with aluminum foils greased with Apiezon-L (Sigma-Aldrich) according to the manufacturer recommendations to prevent the bounce-off of the particles. The two inlets of the system were provided with high-efficiency particulate air (HEPA) filters. The red mud sediment was weighed into a glass flask and was resuspended by intermittent pressure pulses and mechanical shaking. For periods of 20 min, at least five dynamic resuspension episodes were recorded and size distributions were obtained at a resolution of 1 s.

The size distribution and concentration of red mud dust resuspended in the laboratory was also determined using a TSI CPC 3022A condensation particle counter, a GRIMM 1.109 aerosol spectrometer, and a Technoorg APC-01−02 optical particle counter. The initial size range covered by these instruments is between 7 nm (for CPC 3022A) and 32 μm (for GRIMM 1.109). However, since the two optical instruments were calibrated using polystyrene latex particles with a complex refractive index of 1.59 + 0i, whereas the imaginary part of the refractive index of the measured aerosol is ~0.07i, we applied a correction for the size range based on a generalized light scattering model.[12] The corrected size ranges were extended to 18 and 64 μm for the APC and the GRIMM instruments, respectively. The sampling time for all instruments was 1 min, and each measurement was repeated five times.

Mineralogy of the Red Mud Sediment and Resuspended Dust. X-ray powder diffraction (XRD) patterns were obtained

Table 1. Details of Sampling and Types of Analysis Performed[a]

sample no.	location	date	GPS coordinates	description	type of sample (sampler)	types of analysis
1	Kolontár	Oct. 6	47.0819/17.4878	agricultural field covered by red mud	sediment	XRD, SEM
					PM_{10} dust, resuspended in lab (ELPI, AS, OPC, CPC)	SD
					$PM_{(10-1)}$ dust, resuspended in lab (Partisol)	pH
2	Devecser	Oct. 11	47.1018/17.4347	road covered by red mud crust as a result of traffic	$PM_{(10-1)}$ dust, resuspended on site (Partisol)	cc, pH
					PM_1 dust, resuspended on site (Partisol)	cc
3	Devecser	Oct. 11	47.1038/17.4363	sidewalk covered by thin red mud crust	$PM_{(10-1)}$ dust, resuspended on site (Partisol)	cc, pH
					PM_1 dust, resuspended on site (Partisol)	cc
					PM_{10} dust, resuspended on site (MSP)	cc
4	Devecser	Oct. 11	47.1088/17.4351	garden inundated by red mud	sediment	XRD, XRF, SEM
					PM_{10} dust, resuspended in lab (MSP)	m/m%
				driveway inundated by thick mud layer	$PM_{(10-1)}$ dust, resuspended on site (Partisol)	cc, XRD, XRF, SEM, SOSChromo, Flash, ICP-OES, pH
					PM_1 dust, resuspended on site (Partisol)	cc, TEM, ICP-OES
					PM_{10} dust, resuspended on site (MSP)	cc, ICP-OES
5	Somlóvásárhely	Oct. 13	47.1142/17.3856	red mud crust on road as a result of traffic, visible presence of gypsum	$PM_{(10-1)}$ dust, resuspended on site (Partisol)	cc, XRD, SEM
6	Devecser	Oct. 13	47.1088/17.4351	driveway inundated by thick mud layer	$PM_{(10-1)}$ dust, resuspended on site (Partisol)	cc, XRD, SEM, SOSChromo, Flash

[a] ELPI: electrical low-pressure impactor; AS: GRIMM aerosol spectrometer; OPC: Technoorg optical particle counter; CPC: condensation particle counter; MSP: personal aerosol sampler; XRD: X-ray powder diffraction; SEM: scanning electron microscopy, SD: size distribution; ICP-OES: inductively-coupled plasma optical emission spectroscopy; Toxalert, SOSChromo, Flash: various toxicity tests; cc: particle concentration; XRF: X-ray fluorescence spectroscopy; TEM: transmission electron microscopy; m/m%: resuspension potential.

from both red mud sediment and resuspended dust samples using a Philips PW 1710 X-ray diffractometer operated at 50 kV voltage and equipped with a graphite monochromator and a proportional detector. A semiquantitative assessment of the relative concentrations of crystalline phases was performed by modeling XRD patterns using the software CrystalDiffract. X-ray fluorescence spectroscopy (XRF) was used for the analysis of bulk compositions of sediment and $PM_{(10-1)}$ dust samples using a Philips PW 2404 instrument with a Rh anode. Scanning electron microscopy (SEM) was performed on the same samples as XRF for obtaining average red mud sediment and dust compositions and to study particle morphologies. Specimens were prepared by attaching the dried and ground sediment grains to a carbon tape. For higher resolution imaging the sediment and dust grains were mounted on a polished sample holder and coated with Au and Pd. A Philips XL30 SEM with an attached EDAX energy-dispersive X-ray spectrometer was operated at 25-kV accelerating voltage. Transmission electron microscopy (TEM) was performed on resuspended PM_1 dust specimens that were obtained by mounting Cu TEM grids covered with a lacey Formvar+carbon substrate directly onto the backup filter of the Partisol aerosol sampler. Sampling times were less than half a minute in order to avoid the overlap of particles on the collection surface. We used a Philips CM20 electron microscope operated at 200 kV accelerating voltage and equipped with an attached Noran Voyager detector for energy-dispersive X-ray spectroscopy (EDS).

Ecotoxicity. Ecotoxicity assay was performed from the respirable $PM_{(10-1)}$ fraction of the red mud (Table 1). Bioluminescent *Vibrio fischeri* was used as test organism. The light output of bacteria that emit light as a normal consequence of respiration is read by a luminometer. Chemicals or their mixtures that are toxic to the bacteria cause changes in some cellular structures or functions such as the electron transport system, cytoplasmic constituents or the cell membrane, resulting in a reduction in light output proportional to the strength of the toxin. In order to determine the particle-bound, bioavailable toxicity the Flash assay, a kinetic version of the *V. fischeri* bioluminescence inhibition test was performed that was especially developed for assessing the toxicity of solid and/or colored samples.[13,14] Luminescence intensity was evaluated in a kinetic mode: as the bacterial suspension was injected into the sample, the luminous intensity increases resulting in a maximum within 30 s (that is why the system is called Flash). A standardized protocol was followed.[15] Measurements were done in duplicates and were repeated. Toxicity of the samples was assessed using Ascent Software provided by Aboatox Co., Finland.

Genotoxicity. The SOS Chromotest kit (Environmental Bio Detection Products Inc.) was performed on $PM_{(10-1)}$ resuspended dust (Table 1). The analysis followed the protocol provided by the supplier.[16] Freeze-dried bacteria were rehydrated in 10 mL growth medium and incubated overnight at 37 °C. Optical density of the bacteria suspension was measured by a spectrophotometer at 600 nm and the final bacterial concentration was adjusted to the required 0.05 OD_{600} by diluting further with the growth medium. The $PM_{(10-1)}$ dust fraction was suspended in 0.1% DMSO (in 2% NaCl) solution. Samples for genotoxicity were assessed in a 96-well microplate. The first column of the microplate contained the positive control (4-nitroquinoline oxide, 4NQO; six 2-fold serial dilutions in 10% DMSO). Well H in the first column contained 10% DMSO only and served as background control. Columns 2−3 and 4−5 contained the dilutions of the resuspended dust; 14 2-fold dilutions were prepared in 10% DMSO. Each well contained 10 μL aliquot (positive control, background control or red mud dust sample. 100 μL bacterial suspension (OD_{600} = 0.05)) was transferred into each well, and the microplate was incubated at 37 °C for two hours, then 100 μL blue chromogen solution was added to each well and the microplate was incubated at 37 °C for

dx.doi.org/10.1021/es104005r |*Environ. Sci. Technol.* XXXX, XXX, 000–000

Table 2. Results of Various Measurements on the Samples As Listed in Table 1

	concentration (mg m^{-3})			alkalinity (μekv g^{-1})	toxicity of $PM_{(10-1)}$	
sample number	$PM_{(10-1)}$ (Partisol)	PM_1 (Partisol)	PM_{10} (MSP)	$PM_{(10-1)}$	Flash	SOSChromo
1				3.7		
2	36.82	0.95		0.39		
3	23.78	0.41	0.55	0.77		
4	2078.89	24.32	18.27	3.6	no toxicity	no toxicity
5	48.06					
6	2068.3				no toxicity	no toxicity

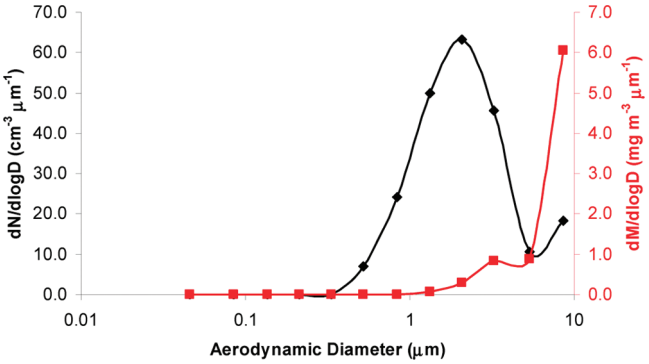

Figure 1. Typical mass and number size distribution of the resuspended red mud dust as determined in laboratory experiments, using an electric low-pressure impactor (ELPI).

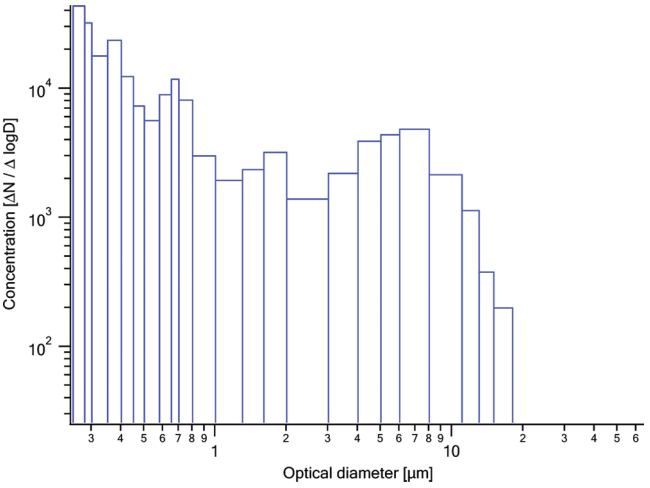

Figure 2. Typical number size distribution of the resuspended red mud dust as determined in laboratory experiments, using an optical particle spectrometer. The number concentration on the graph is displayed in [number/liter/μm].

90 min. Finally, 50 μL alkaline phosphatase was added to each well and the microplate was incubated 37 °C for one hour. Sequential activities of β-galactosidase (indicating genotoxic activity by a blue color) and alkaline phosphatase (indicating viability of the bacteria by yellow color) were assessed visually.

RESULTS

Resuspension Potential, Alkalinity, Metals. The resuspended PM_{10} fraction of dried and pulverized red mud sediment was 0.99 m/m% (standard deviation 0.19). The concentration of $PM_{(10-1)}$ strongly depended on the amount of red mud that was available for resuspension, as reflected by the highly variable concentrations measured in our field experiments (Tables 1 and 2). Concentrations were 2 orders of magnitude larger when dust was resuspended from a driveway that was covered by a thick (~1 cm) layer of mud (samples 4 and 6) than in cases when only a thin crust of mud covered the pavement (samples 2, 3, and 5) (Table 2).

The specific alkalinity of the $PM_{(10-1)}$ fraction of resuspended dust was 3.7 μekv g^{-1}. A similar result (3.6 μekv g^{-1}) was obtained from a sample collected from an inundated surface. It should be noted that lower alkalinity was determined for samples collected from surfaces that were indirectly affected by red mud as a result of traffic (Table 2). The specific alkalinity of the PM_1 fraction could not be determined directly, but it was likely higher due to the higher specific surface area of fine particles. The concentrations of the measured metals (Cd, Co, Cu, Ni) were below the detection limit (10 ppb).

Size Distribution. The mass size distribution of resuspended red mud dust is bimodal (Figure 1), as measured using the ELPI. Most of the mass is concentrated at or above the aerodynamically equivalent diameter (AED) of 10 μm, with a smaller secondary mode around 4 μm. The number size distribution is dominated by particles with diameters of about 2 μm.

The typical number size distribution of the red mud aerosol measured by optical instruments is shown in Figure 2 and exhibits a pronounced peak in the range between optical diameters of 3 and 8 μm. The concentration of particles with diameters <1 μm measured by the condensation particle counter was not considerably larger than those measured by the optical instruments (Grimm and APC) for the same size range, indicating that the concentration of particles with sizes below the detection limit of optical particle counters is relatively small. The size distribution measurements based on two different principles gave broadly consistent results: the mean optical diameters are close to the observed mean geometrical diameters (as estimated from TEM images), whereas aerodynamically equivalent diameters could well differ from the geometrical ones if the density of the particles is much different from unity and their shapes are far from being spherical. On the other hand, AED is more relevant in determining how particles behave in the human respiratory system.

Toxicity Measurements. In our assays, no direct toxicity was detected. For comparative purposes, the toxicity of three PM_{10} aerosol samples collected in Budapest (Hungary) in January 2010 was also assessed using the Flash assay. EC_{50} of

dx.doi.org/10.1021/es104005r |Environ. Sci. Technol. XXXX, XXX, 000–000

Table 3. Minerals Identified in Red Mud Sediment and Dust Samples and Their Likely Origins

mineral identified by XRD and/or TEM	nominal composition	probable origin
hematite	Fe_2O_3	bauxite
cancrinite	$Na_6CaAl_6Si_6(CO_3)O_{24} \cdot 2H_2O$	alumina production
"hydrogarnet"	$Ca_3AlFe(SiO_4)(OH)_8$	alumina production
calcite	$CaCO_3$	bauxite or alumina production
perovskite	$CaTiO_3$	bauxite
boehmite	$AlO(OH)$	bauxite
gibbsite	$Al(OH)_3$	bauxite or alumina production
quartz	SiO_2	bauxite or soil
albite	$NaAlSi_3O_8$	soil
muscovite	$KAl_2(AlSi_3O_{10})(OH)_2$	soil
rutile	TiO_2	bauxite
gypsum	$CaSO_4 \cdot 2H_2O$	cleanup procedures

the samples varied between 0.064 and 0.23 mg mL^{-1} suspension, indicating that "whole-aerosol" toxicity testing in principle can be sensitive to detect the environmental risk of the bioavailable fraction of aerosols.

Mineralogy of the Red Mud. The red mud sediment and the resuspended $PM_{(10-1)}$ dust contain the same crystalline substances, according to the results of XRD analyses (Table 3). The solid phases may originate from three distinct sources: (1) they were originally present in bauxite and survived the alkaline leaching; (2) they formed in the course of the Bayer process; (3) they were mobilized from the soil by the tsunami-like surge of the sludge.

The composition of red mud depends on the type of bauxite and thus can be highly variable.[17−19] Hematite is a major mineral component of all Hungarian and Mediterranean karst bauxite types [17] that may have been processed in the Ajka plant since 2001, during the operation of the breached red mud reservoir. Other residual bauxite minerals could include boehmite and gibbsite, the Ti minerals perovskite and rutile, and calcite. Quartz can be present in a small amount in bauxite as a detrital mineral, but may also have originated from the soil. The typical silicate components of the red mud are technological byproducts of the Bayer process [20] and include cancrinite and a hydrogarnet-like phase that has no known natural analog and thus does not have a mineral name. Since both silicate phases can have highly variable compositions owing to various cation substitutions in their structures,[21] idealized formulas are shown in Table 3. Albite, muscovite, and the majority of quartz were presumably mobilized from the soil. In one of the dust samples gypsum is present that was used in large quantities in the cleanup efforts with the aim of binding the fine-grained particles of red mud. Some of the smaller peaks in the experimental XRD patterns could not be adequately simulated using model mixtures of the phases in Table 3.

A semiquantitative assessment of XRD patterns reveals that the major components of red mud are hematite, cancrinite, calcite, and hydrogarnet (Figure 3). A comparison of samples 4 and 6a (that can be regarded as most representative of "clean" red mud sediment and $PM_{(10-1)}$ dust, respectively) reveals that hematite, cancrinite, and hydrogarnet are only slightly enriched

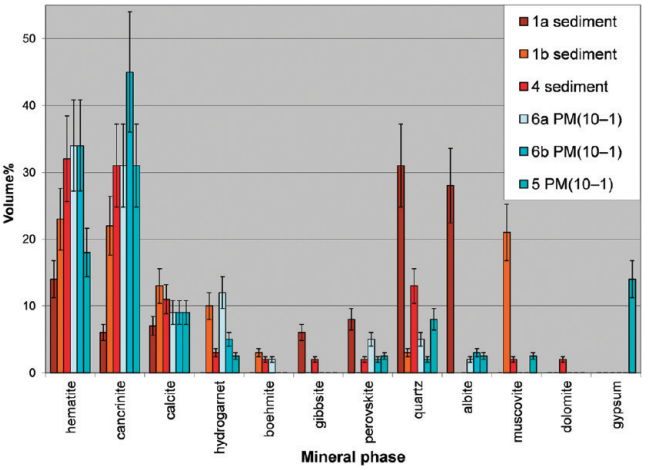

Figure 3. Comparison of the mineralogical compositions of red mud sediment (samples 1a, 1b, and 4) and $PM_{(10-1)}$ resuspended dust (samples 6a, 6b, and 5), as determined from X-ray powder diffractograms. Whereas the relative amounts of the major mud constituents (hematite, cancrinite, calcite, hydrogarnet) are similar in the sediment and $PM_{(10-1)}$ samples, the sediment samples contain a larger percentage of soil-derived minerals (quartz, albite, muscovite) than the dust samples.

in the dust relative to the sediment. The relative amount of soil-derived minerals (quartz, albite, muscovite) and of calcite is larger in the sediment samples than in the $PM_{(10-1)}$ dust, especially in the case of sample 1 that was collected on a field. Presumably, the grain sizes of soil minerals are larger than those of red mud particles, and are thus less likely to become airborne.

The bulk chemical compositions of the samples were analyzed using XRF (Figure 4). The concentrations of analyzed elements are essentially identical in the sediment and $PM_{(10-1)}$ dust samples. A slight enrichment of Fe in the $PM_{(10-1)}$ dust is consistent with the enhanced hematite concentration that was determined by XRD. Similarly higher concentrations of Ti, V, Cr, and Ni were observed; these metals likely substitute for Fe in hematite. The minor enrichment of Na and Al in the dust might result from the slightly enhanced concentrations of cancrinite and hydrogarnet, whereas the lower amount of Ca and Si is consistent with the smaller concentrations of calcite and quartz in the $PM_{(10-1)}$ dust relative to the sediment.

The sizes of individual particles in the $PM_{(10-1)}$ fraction of resuspended dust were measured on SEM images. The resulting size distribution is log-normal with a mean diameter at 4.4 μm (SI Figure SI 2). In secondary electron images most particles appear as fluffy aggregates, although larger crystals with euhedral and layered habits also occur (Figure 5). "Bulk" compositions determined from EDS analyses of large sample areas (3 × 0.5 cm^2) are very similar to those obtained with XRF (SI Figure SI 3). On the other hand, the compositions of individual particle aggregates are highly variable, suggesting that the relative ratios of the major mineral components (hematite, cancrinite, calcite, hydrogarnet) vary between individual particles (SI Figure SI 4).

TEM images confirm the results of particle size measurements: in the PM_1 fraction the geometrical diameters of particles range from ~0.2 to 3 μm. The shapes of the individual particles are irregular, typically angular, and they produce heterogeneous contrast in bright-field images (SI Figure SI 5). Higher-magnification images (Figure 6) show that each aerosol particle is an aggregate of a large number of nanocrystals (SI Figure SI 6).

dx.doi.org/10.1021/es104005r |Environ. Sci. Technol. XXXX, XXX, 000–000

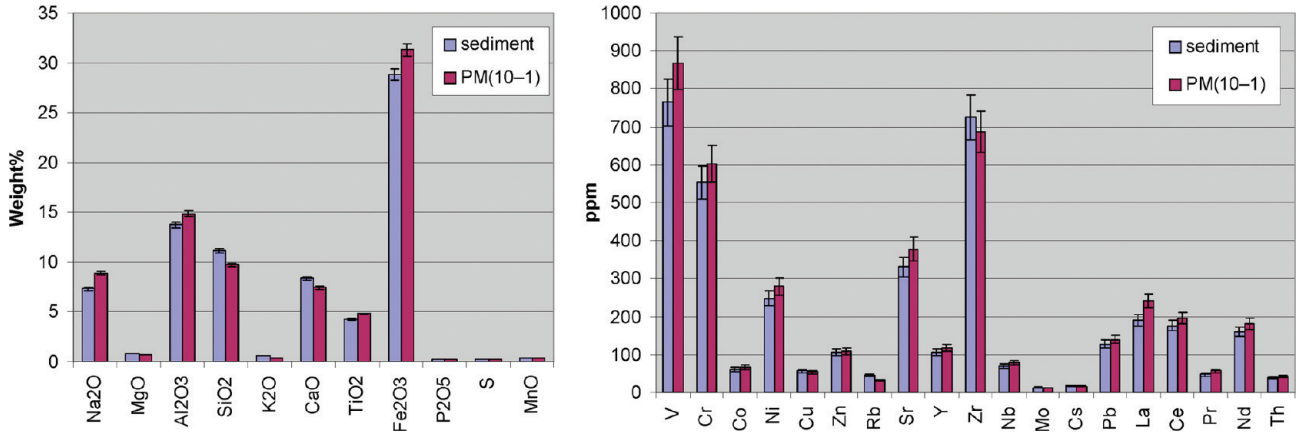

Figure 4. Comparison of the chemical composition of red mud sediment and $PM_{(10-1)}$ resuspended dust (sample 4), as determined from X-ray fluorescence spectrometry.

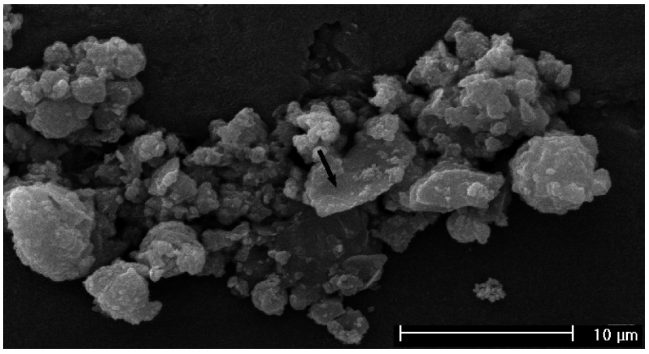

Figure 5. SEM image of the $PM_{(10-1)}$ fraction of resuspended red mud dust (sample 4). Most particles are fluffy aggregates with diameters smaller than ~5 μm. Some flake-like crystals (marked by the arrow) also occur.

According to SAED patterns, randomly oriented hematite nanocrystals are a major component of virtually every particle (SI Figure SI 5). The hematite crystals are typically euhedral, equant or slightly elongated, and their sizes range from ~10 to 100 nm (Figure 6). EDS spectra obtained from both entire particles and their individual crystalline components reveal that Ti substitutes for ~5% of Fe in hematite.

Both cancrinite and hydrogarnet appear in the form of thin, platy, or lamellar crystals (Figure 6a). When exposed to an intense electron beam, both minerals suffer visible damage, probably resulting from the release of volatile constituents such as H_2O, OH^-, CO_3^{2-}, and Na^+ from their structures (SI Figure SI 7). The flaky silicate minerals appear to provide suitable surfaces for the adsorption of the smaller hematite nanocrystals. Thus, each individual dust particle is a complex mixture of the major mineral components of red mud. However, the ratios of these minerals vary strongly from one particle to the other, as indicated by EDS spectra that were obtained from entire individual particles (SI Figure SI 8).

DISCUSSION

An assessment of potential health effects of fugitive dust should consider a number of aspects that are related to the special properties of red mud, including its particle size distribution, highly alkaline character, and the potential toxicity of red mud itself and its constituents.

Resuspension Potential. The extremely high potential resuspension ratio (nearly 1 m/m%) is unprecedented among natural soils which usually have their value in the ppm range.[22] This high resuspension potential of red mud sediment is confirmed in the field sampling tests in which the measured flux of resuspended $PM_{(10-1)}$ from an inundated paved surface was about 200 times higher (samples 4 and 6, Table 2) than that observed when the same sampling apparatus was used at kerbside locations in the city of Veszprém.

Size Distribution Vs Respirability. The typical mass size distribution of urban aerosol is bimodal, with one distinct peak in the 0.1−1 μm range (accumulation mode), and another in the 1−10 μm range (coarse mode).[23] Particles in the coarse mode may originate from erosion, wind dispersion of road and soil dust and anthropogenic activities, for example the thermal- and motion-induced mobilization of road dust and vehicle emissions (from the abrasion of tires and brakes).[23,24] The elements that presumably originate form the Earth's crust (Al, Si, Ca, Ti, and Fe) are typically associated with a single size mode with geometric mean aerodynamic diameters of 4−5 μm.

This mode almost perfectly matches the small secondary mode in the measured mass size distribution of red mud dust particles (see Figure 1). The maximum local deposition of inhaled particles in this mode occurs in the extrathoracic region of the respiratory tract with a mean depositional rate of about 70−80%.[25] Thus, most coarse particles in this size range are already trapped in nasal passages and do not enter the lungs. Fortunately, the nucleation (ultrafine) mode (particles with AED <0.1 μm) of urban aerosol that is the most critical in terms of health effects is completely missing from the mass size distribution of fugitive dust of red mud. If present, this fraction would get all the way through the alveoli and deposit with high efficiency there. Particulate matter in the accumulation mode range, being absent from red mud dust but a major fraction of urban PM_{10}, also has serious health implications in urban air in spite of the fact that its total depositional rate is rather low (<25%) in the entire respiratory system. The severe health effects of particles of this size are due to their high mass concentrations in polluted urban air as well as a plethora of toxic, mutagenic, carcinogenic compounds that result from combustion or other anthropogenic activities, or form in photochemical processes.[26] The dominant

dx.doi.org/10.1021/es104005r |Environ. Sci. Technol. XXXX, XXX, 000–000

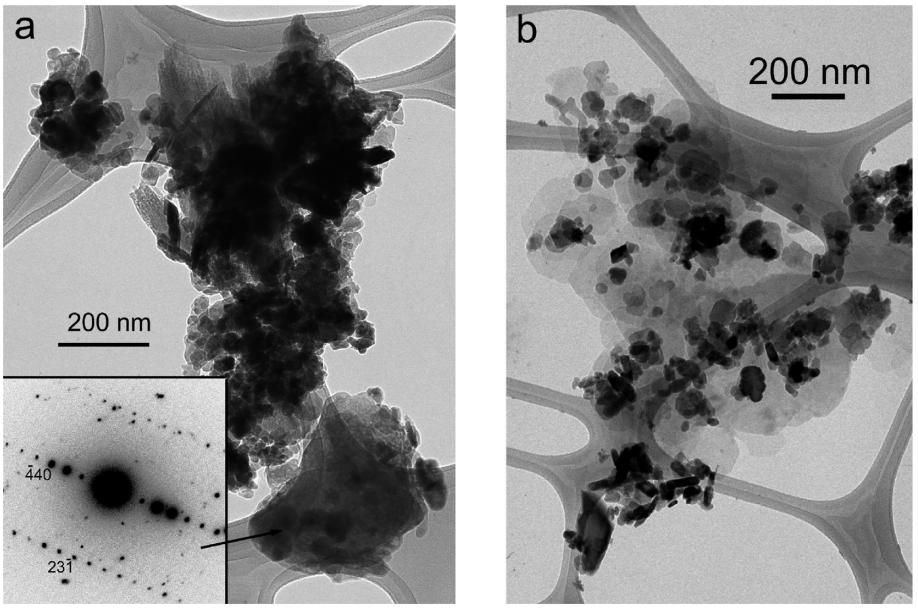

Figure 6. TEM images of typical particle aggregates in the PM_1 fraction of resuspended red mud dust. Euhedral and subhedral nanocrystals with dark contrast are hematite particles, whereas the flaky, lighter-contrast grains are silicates. (a) The SAED pattern in the inset indicates that the arrowed crystal is cancrinite. (b) Hematite nanocrystals are attached to silicates that appear to form thin layers.

size fraction in red mud dust (Figure 1) that is typically much less significant in urban air [27] except for special locations and/or circumstances,[28] has only extrathoracic deposition. It means that this fraction—no matter how large its concentration—can cause irritation of "only" the upper respiratory tract (and the eyes).

Potential Health Effects of Alkalinity. A comprehensive survey on the health effects of respiration of caustic mist was conducted involving nearly 2500 employees of three alumina factories.[29] Subjects exposed to the highest levels of caustic mist (>1 mg m^{-3} expressed in mass concentrations of pure NaOH) showed somewhat elevated prevalence of wheeze and rhinitis, but no change was detected in their lung function. Thus, a recommended ceiling level of 1 μg m^{-3} for pure NaOH was adopted by the European Chemicals Bureau in 2007.[9] Since the NaOH-equivalent concentration of red mud dust, as calculated from the measured alkalinity, is only 0.001 μg m^{-3} at the health limit value of total PM_{10} (50 μg m^{-3}), the inhaled alkalinity from red dust is well below the recommended no-effect limit. Since even pure NaOH did not induce mutagenicity in reported long-term in vitro and in vivo studies,[9] the alkalinity of the red mud dust is unlikely to cause severe acute or chronic symptoms in healthy adults. Unfortunately, little is known about how other groups of the population (e.g., infants, children, elderly people, people with cardiovascular or respiratory illnesses) are affected by the alkalinity of the dust. Eye irritation was reported by residents of the affected area and workers involved in the cleanup in the weeks immediately following the spill.

Potential Health Effects of Red Mud Dust Constituents. In the investigated dilution range of the red mud dust samples, no genotoxic activity was detected in the $PM_{(10-1)}$ airborne fraction. Brunori et al. [6] also applied the *V. fischeri* bioluminescence inhibition test (Microtox) to estimate the toxicity of the bauxite residue from the Eurallumina plants located in Sardinia (Italy) and found that every value was below the detection limit of the test system. A 10-year-long study by Dauvin [7] also used the Microtox system and assessed the environmental impact of red mud directly discharged to the Cassidaigne canyon (northwestern Mediterranean Sea, Marseilles area, France). With the exception of a direct contact test, organic extracts, interstitial water samples, lixiviated samples and whole sediments were nontoxic in all cases.[7,30] Nevertheless, we stress that such ecotoxicity test (including ours in this study) are primarily useful for assessing only environmental (and not human) health effects.

The major minerals of the red mud are hematite, cancrinite, calcite, and hydrogarnet. Calcite is a common mineral that is unlikely to cause any adverse health effects. Although there is a large body of literature on the health effects of silicate minerals that occur in asbestiform varieties,[31] we are not aware of any studies on the effects of cancrinite and hydrogarnet. Both minerals occur in red mud as platy, lamellar crystals. Thus, the fibrous habits that have been thought to be associated with the carcinogenic effects of some asbestiform silicates are absent.

The effects of inhaled hematite dust have been studied in the case of iron ore miners.[32] Among hematite miners in China a significant excess risk of nonmalignant respiratory disease and of lung cancer was found.[33] However, a heavy exposure to radon, quartz dust, and diesel fumes in unventilated underground mines probably contributed to the high mortality of the miners, and the independent effects of exposure to hematite dust could not be evaluated. Another study found no apparent health risks associated with hematite mining;[34] in this study the miners were not exposed to significant radon concentrations, smoking was prohibited underground and diesel emissions were also absent. Roentgenologic changes in the lung due to the deposition of inhaled iron-bearing particles is called siderosis and was observed in many occupational groups exposed to iron oxide fumes. These changes of the lungs are generally regarded to be benign without having any influence on lung function or progressing to fibrosis.[35]

Concerning the presence of transition metals other than Fe in the dust, we did not detect any alarmingly large concentrations using XRF (see Figure 4). EDS analysis of ~40 individual particles in the TEM suggest that transition metals other than Fe (such as Ti, Mn and Cr) are incorporated into the hematite structure (SI Figure SI 8). Thus, apart from the large resuspension

potential and consequently large atmospheric concentrations under windy conditions, the fugitive dust from red mud does not appear to pose a serious health hazard for residents of the affected region. We recommend, however, that persons involved in decontamination efforts or agricultural activities wear protective masks when meteorological conditions result in dry red mud surfaces.

■ ASSOCIATED CONTENT

Supporting Information. Scanning and transmission electron microscopy images, electron diffraction patterns and energy-dispersive X-ray analyses show the sizes, morphologies, crystal structures, and compositions of airborne particles of red mud. This material is available free of charge via the Internet at http://pubs.acs.org.

■ AUTHOR INFORMATION

Corresponding Author

*Phone: +3688624155; fax: +3688624454; e-mail: mihaly.posfai@gmail.com.

■ ACKNOWLEDGMENT

We thank four anonymous reviewers for their rapid work and constructive comments on the first version of this manuscript. The financial support of NKFP grant No. AEROSOL_EU 2004/3A089 is gratefully acknowledged.

■ REFERENCES

(1) Johnston, M.; Clark, M. W.; McMahon, P.; Ward, N. Alkalinity conversion of bauxite refinery. *J. Hazard. Mater.* **2010**, *182* (1−3), 710–715.

(2) Niculescu, M.; Ionita, A. D.; Filipescu, L. Chromium adsorption on neutralized red mud. *Rev. Chim. (Bucharest, Rom.)* **2010**, *61* (2), 200–205.

(3) Summers, R. N.; Guise, N. R.; Smirk, D. D. Bauxite residue (red mud) increases phosphorus retention in sandy soil catchments in Western Australia. *Fert. Res.* **1993**, *34* (1), 85–94.

(4) Yadav, V. S.; Prasad, M.; Khan, J.; Amritphale, S. S.; Singh, M.; Raju, C. B. Sequestration of carbon dioxide (CO_2) using red mud. *J. Hazard. Mater.* **2010**, *176* (1−3), 1044–1050.

(5) Hind, A. R.; Bhargava, S. K.; Grocott, S. C. The surface chemistry of Bayer process solids: A review. *Colloid Surf., A* **1999**, *146* (1−3), 359–374.

(6) Brunori, C.; Cremisini, C.; Massanisso, P.; Pinto, V.; Torricelli, L. Reuse of a treated red mud bauxite waste: Studies on environmental compatibility. *J. Hazard. Mater.* **2005**, *117* (1), 55–63.

(7) Dauvin, J.-C. Towards an impact assessment of bauxite red mud waste on the knowledge of the structure and functions of bathyal ecosystems: The example of the Cassidaigne canyon (north-western Mediterranean Sea). *Mar. Pollut. Bull.* **2010**, *60* (2), 197–206.

(8) Samet, J. M.; Dominici, F.; Curriero, F. C.; Coursac, I.; Zeger, S. I. Fine particulate air pollution and mortality in 20 US cities 1987−1994. *New Eng. J. Med.* **2000**, *343*, 1742–1749.

(9) European Chemicals Bureau, *Sodium hydroxide*, Ispra, pp CAS No: 1310−73−2; 2007; 215-185−5.

(10) Watanabe, T.; Hirayama, T. Genotoxicity of soil. *J. Health Sci.* **2001**, *47* (5), 433–438.

(11) Ruyters, S.; Mertens, J.; Vassilieva, E.; Dehandschutter, B.; Poffijn, A.; Smolders, E. The red mud accident in Ajka (Hungary): plant toxicity and trace metal bioavailability in red mud contaminated soil. *Environ. Sci. Technol.* [Online early access] DOI: 10.1021/es104000m. Published Online: January 4, **2011**.

(12) Gouesbet, G.; Lock, J. A.; Gréhan, G. Generalized Lorenz-Mie theories and description of electromagnetic arbitrary shaped beams: Localized approximations and localized beam models, a review. *J. Quant. Spectrosc. Radiat. Transfer* **2011**, *112* (1), 1–27.

(13) Lappalainen, J.; Juvonen, R.; Vaasajari, K.; Nurmi, J.; Karp, M. A new flash method for measuring toxicity of solid and colored samples. *Chemosphere* **1999**, *38* (5), 1069–1083.

(14) Lappalainen, J.; Juvonen, R.; Nurmi, J.; Karp, M. Automated color correction method for *Vibrio fischeri* toxicity test. Comparison of standard and kinetic assays. *Chemosphere* **2001**, *45*, 635–641.

(15) *Water Quality - Kinetic Determination of the Inhibitory Effects of Sediment and Other Solids and Coloured Samples on the Light Emission of Vibrio fischeri /Kinetic Luminescent Bacteria Test/*, ISO 21338, 2010.

(16) EBPI. *The SOS-Chromotest Kit Version 6.4. Instructions for Use*; Environmental Biodetection Products Inc.: Mississauga, Ontario Canada, 2009.

(17) Bárdossy, G. Karst Bauxites. *Bauxite Deposits on Carbonate Rocks*; Elsevier: Amsterdam, 1982; p 441.

(18) Zhang, Y.; Qu, Y.; Wu, S. Engineering geological properties and comprehensive utilization of the solid waste (red mud) in aluminium industry. *Environ. Geol.* **2002**, *41* (3−4), 249–256.

(19) Gräfe, M.; Power, G.; Klauber, C. *Review of Bauxite Residue Alkalinity and Associated Chemistry*; CSIRO Document DMR-3610; CSIRO: Clayton South, Victoria Australia, 2009.

(20) Suss, A. G.; Kuvyrkina, A. M.; Kuznetsova, N. V.; Panov, A. V. Effect of sodium hydroaluminosilicate (SHAS) structure on removal of impurities from alumina production solutions and on efficiency of regeneration processes. *Metallurgist* **2008**, *52* (11−12), 653–656.

(21) Della Ventura, G.; Gatta, G. D.; Redhammer, G. J.; Bellatreccia, F.; Loose, A.; Parodi, G. C. Single-crystal polarized FTIR spectroscopy and neutron diffraction refinement of cancrinite. *Phys. Chem. Mineral.* **2009**, *36* (4), 193–206.

(22) Young, T. M.; Heeraman, D. A.; Sirin, G.; AshBaugh, L. L. Resuspension of soil as a source of airborne lead near industrial facilities and highways. *Environ. Sci. Technol.* **2002**, *36*, 2484–2490.

(23) Salma, I.; Balásházy, I.; Winkler-Heil, R.; Hoffmann, W.; Záray, G. Effect of particle mass size distribution on the deposition of aerosols in the human respiratory system. *Aerosol Sci.* **2002**, *33*, 119–132.

(24) Salma, I.; Ocskay, R.; Raes, N.; Maenhaut, W. Fine structure of mass size distributions in an urban environment. *Atmos. Environ.* **2005**, *39*, 5363–5374.

(25) Salma, I.; Maenhaut, W.; Záray, G. Comparative study of elemental mass size distributions in urban atmospheric aerosol. *Aerosol Sci.* **2002**, *33*, 339–356.

(26) Gelencsér, A. *Carbonaceous Aerosol*. Springer: Berlin, Heidelberg, NY, 2004.

(27) Grobéty, B.; Gieré, R.; Dietze, V.; Stille, P. Airborne particles in the urban environment. *Elements* **2010**, *6*, 229–234.

(28) Chen, W.; Fryrear, D. W. Sedimentary characteristics of a haboob dust storm. *Atmos. Res.* **2002**, *61*, 75–85.

(29) Fritschi, L.; De Klerk, N.; Sim, M.; Benke, G.; Musk, A. W. Respiratory morbidity and exposure to bauxite, alumina, caustic mist in alumina refineries. *J. Occup. Health* **2001**, *43*, 231–237.

(30) Ribera, D.; Saint-Denis, M. Evaluation des dangers et gestion des risques. Quelques perspectives en écotoxicologie animale. *Bull. Soc. Zool. Fr.* **2002**, *127*, 329–341.

(31) Guthrie, G. D.; Mossman, B. T. *Health Effects of Mineral Dusts*; Mineralogical Society of America: Washington, DC, 1993.

(32) Ross, M.; Nolan, R. P.; Langer, A. M.; Cooper, W. C. Health effects of mineral dusts other than asbestos. *Rev. Mineral.* **1993**, *28*, 361–407.

(33) Chen, S. Y.; Hayes, R. B.; Liang, S. R.; Li, Q. G.; Stewart, P. A.; Blair, A. Mortality experience of haematite mine workers in China. *Brit. J. Ind. Med.* **1990**, *47* (3), 175–181.

(34) Lawler, A. B.; Mandel, J. S.; Schuman, L. M.; Lubin, J. H. A retrospective cohort mortality study of iron ore (hematite) miners in Minnesota. *J. Occup. Med.* **1985**, *27* (7), 507–517.

(35) Morgan, W. K. C. Occupational lung disease. In *Merck Manual of Medical Information*, 2nd Home Online ed.; Beers, M. H. e. a., Ed.; Pocket Books: New York, 1997; 195−201.